Microsyst Technol (2013) 19:1289–1306
DOI 10.1007/s00542-013-1785-0

TECHNICAL PAPER

A fast battery charging algorithm for an intelligent PV system with capability of on-line temperature compensation

Paul C.-P. Chao · Wei-Dar Chen · Chun-Wei Cheng

Received: 31 October 2012 / Accepted: 17 March 2013 / Published online: 29 March 2013

Abstract This study presents a battery fast-charging mechanism for an intelligent generic photovoltaic (PV) system and also a pulse-charging method for the on-line temperature compensation. The fuzzy logic control (FLC) is adopted for fast maximum power point tracking (MPPT) of the PV system. Along with proposed battery charging algorithms, the controller presented in this study is named a fuzzy battery-managing controller (FBMC). The fast battery charging by this controller does not only prolong battery lifetime by restoring the maximum battery state of charge (SOC) in the shortest time but also with the temperature compensation. The designed charging algorithm consists of three different stages, namely constant current (CC), pulse charging and trickle charging. In the CC mode, the current at maximum power of the PV array is used for fast charging. The pulse charging mode is next adopted to contain temperature rise while maintaining relatively fast charging speed. To prevent battery damage by charging as battery capacity is close to its full status, 100 % SOC, the float charging mode is finally activated by further decreasing charging currents. Simulations are conducted via Powersim to validate the FBMC performance and the PV system model. The FBMC is next implemented by a DSP module (TMS320F2812) in order to adjust the switching duty cycle during operations of the buck converter. Finally, experimental results were compared with a general constant current and/or voltage method. The results show favorable performance of the propose charging method.

P. C.-P. Chao (✉) · W.-D. Chen · C.-W. Cheng
Department of Electrical Engineering, National Chiao Tung University, Hsinchu 300, Taiwan
e-mail: pchao@mail.nctu.edu.tw

P. C.-P. Chao
Institute of Imaging and Biomedical Photonics, National Chiao Tung University, Tainan 711, Taiwan

1 Introduction

Renewable energies have, as one of clean energies, become one viable candidate to replace traditional fossil fuel. Renewable energy comes from natural resources, such as wind power energy, hydro energy, biomass energy, geothermal energy, ocean energy and photovoltaic (PV) energy. Among aforementioned renewable energies, the photovoltaic (PV) energy is expected to be a major clean energy source without pollution and energy waste due to accessibility of solar energy and relative simplicity involved in the manufacture, structure and electronics of a PV array. A PV system is always along with DC–DC converters and energy storage device. The energy is converted into a suitable and stable voltage to the back-end system by converters. The storage device is usually used to storage or provide energy to the load.

In a typical PV system, there is a DC–DC converter (Veerachary 2011; Ta-Tau et al. 2011), which is designed responsible for extracting power out of the front-end PV panel. The function of this DC–DC converter is to adjust its impedance seen by the PV panel to be close to the corresponding impedance of the PV panel, thus maximizing the output efficiency via impedance matching (Xiao et al. 2007). The combination of corresponding current and voltage of the PV panel is so-called the maximum power point (MPP) in the characteristic curve–voltage curves. Many methods and controllers have been developed to track the MPP like as methods of power feedback control (Al-Atrash et al. 2005), perturb and observe (P&O) (Santos et al. 2006; Elgendy et al. 2012; Joe-Air et al. 2005) or

incremental conductance (Kish et al. 2012; Azimi et al. 2012). These control schemes suffer different drawbacks during MPPT; for instance, the P&O has oscillation problem. Therefore, other intelligent control methods like fuzzy logic or neural network were introduced in (Paul et al. 2012; Chian-Song 2010; Agorreta et al. 2009; Bouchafaa et al. 2011; Salah and Ouali 2011; Taherbaneh and Faez 2007). In this study, an intelligent MPPT with different and more efficient converter, membership function and rule table is designed and achieved by a buck converter with a fuzzy battery-managing controller (FBMC).

The lithium-ion battery in the system is used to store energy in the PV system generally (Reynaud et al. 2010). A high working voltage, high power and energy density, low self discharge rate and no memory effect are all the advantages of the lithium-ion battery (Yuang-Shung and Ming-Wang 2005). The over-charge/discharge and temperature of battery are the main problems of battery management (Kularatna 2010). The constant current and/or voltage (CC/CV) charging is widely applied to achieve battery state of charge (SOC) (Fakham et al. 2011). Note that the SOC is not only presents the battery condition but also affects its life. The general CC/CV method cannot be reached or not even close to the 100 % SOC. This study proposes a fast battery charging algorithm that is not only increasing the battery lifetime by restoring the maximum available battery SOC in the shortest time but also with the temperature compensation. The method of floating charge is adopted to reach 100 % SOC condition by finally overcharging at a *C*/100 charge rate (Koutroulis and Kalaitzakis 2004), while the pulse charging method (Huria et al. 2012) is employed to avoid undesired temperature rise. To the end of temperature compensation, a thermal couple is used to provide on-line temperature feedbacks (Szumanowski and Yuhua 2008) for regulate charging current and adjusting related parameters.

Simulations are conducted using Powersim to validate the FBMC performance and the PV system model. The FBMC is next implemented by a DSP module (TMS320F2812) in order to adjust the switching duty cycle during operations of the buck converter. Finally, experimental results were compared with general CC/CV charging method. The results show favorable performance of the propose charging method.

The remainder of this study is organized as follows. Section 2 establishes the designed PV system and determine of passive components used in the buck converter. Section 3 analyzes and establishes a temperature compensation of battery model and the designed charge method. Section 4 provides the design processes and details of the FBMC controller. In Sect. 5, the performance of designed system is simulated by Powersim to confirm the effectiveness of the designed FBMC controller in enabling a fast and smooth MPPT. Experimental setup and results are also given in this section to validate the controller performance. Finally, Sect. 6 provides brief concluding remarks and intended directions for future research work.

2 System description and design

2.1 System description

A intelligent photovoltaic (PV) system as shown in Fig. 1 with capability of battery fast charging is considered in this study. The system consists of a PV array, a buck converter and a lithium-ion battery. The power switches of the buck converter are controlled by the gate drivers programmed via a DSP module. The converter delivers required levels of power output to the rear-end power grid or a battery. The buck converter is responsible for MPPT and battery charging voltage/current.

The equivalent circuit of the considered PV array is shown in Fig. 2, where the PV array is modeled by a parallel connection of a current source I_{sc}, a diode, an internal parallel and series resistances, R_{sh} and R_S. The relationship between the current and the voltage of the PV array V_{pv} can be well prescribed by (Kwon et al. 2006)

$$I_{pv} = I_{sc} - I_s\left[\exp\left(\frac{q(V_{pv}+I_{pv}R_s)}{AKT}\right)-1\right]-\frac{V_{pv}+I_{pv}R_s}{R_{sh}}, \quad (1)$$

where I_{pv} is the output current of the PV array; I_s is the reverse saturation current; q is the charge of an electron (1.6×10^{-19} C); K is the Boltzmann's constant; A is the ideality factor of the p–n junction; T is the temperature (deg K) of the PV array. The irradiation and temperature influence the output power in a nonlinear relation at every moment. The characteristics curves for I–V and P–V relations of the PV array can be simulated by a commercial software Powersim with Eq. (1). Figure 3 displays typical simulation results for different energy densities at the PV array. It is evident from this figure that under the different irradiation and temperature conditions, the maximum power pint (MPP) is changed. It means that the MPP is a time-varying parameter. This makes the maximum power point tracking (MPPT) a difficult task.

Various techniques to achieve an on-line, dynamic MPPT have been reported by researchers. The most common one is the Perturb and Observation (P&O) method (Santos et al. 2006; Elgendy et al. 2012; Joe-Air et al. 2005), due to its simplicity and ease to achieve MPPT. The method proposes four simple tuning rules on the duty for different polarity combinations of changes in power and voltage of the PV array. The tuning increment on the duty is however fixed. Therefore, the time span required to reach

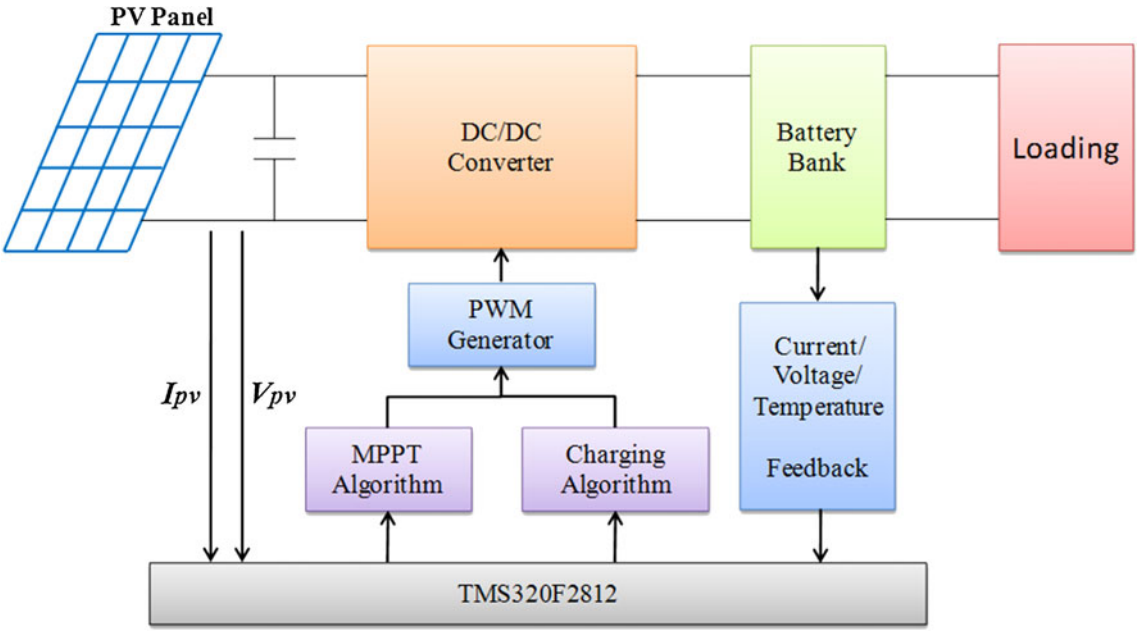

Fig. 1 The proposed intelligent photovoltaic system

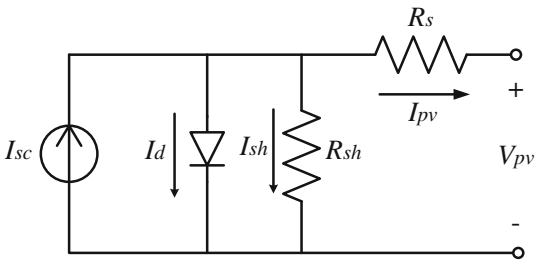

Fig. 2 The equivalent circuit of the photovoltaic array

MPPT is relatively long, not to mention the difficulty for the tracker to stay right on the MPP since each time the perturbation on tuning the voltage is finite. To tackle the aforementioned disadvantage, some intelligent control methods were developed recently (Paul et al. 2012; Chian-Song 2010; Agorreta et al. 2009; Bouchafaa et al. 2011; Salah and Ouali 2011). In this study, a fuzzy logic controller (FLC) is designed, which make possible a varying increment for the output duty. The increment is determined by the fuzzy mechanism. This aims to realize a fast, smooth and accurate MPPT. The designed FLC control algorithm consists mainly of four parts as fuzzification, rule base, fuzzy inference engine and defuzzification. The input signals experiences fuzzification, interference rules and finally defussification. The interference rules could follow the same deterministic rules adopted by the conventional P&O method, a flow-chart representation of which is given in Fig. 4. The design details of the controller is given in Sect. 4.

2.2 Determining inductance and capacitance

With the traditional converter technology, effort is dedicated herein to determine inductance and capacitance of the designed buck DC–DC converter. Design of a DC–DC buck converter is basically intended to convert the original DC input to a steady output DC voltage in another level (Mohan et al. 2003). The designation of passive devices in this converter is carried out by first considering two equivalent circuits as shown in Fig. 5, two topologies of which refers to different cases with switch on and off. The MPP of the PV array is achieved when the input resistance of the converter equal to the equivalent output resistance of the PV panel (Impedance matching). The equivalent circuit is shown in Fig. 6. Following a standard procedure of analysis via the conversion between continuous and discrete representations of the inductance current, as given in (Mohan et al. 2003), one can obtain the output voltage simply equal to

$$V_{out} = D \cdot V_{in}, \tag{2}$$

where V_{in} is the input voltage of converter; V_{out} is the output voltage of converter; D is the duty cycle of the switch and varied between [0.1, 0.9]. The output voltage is successfully reduced to a lower level. The analysis thus far is based on the assumption that the inductance current is continuous, the inductance L can be described as

$$L > \frac{(V_{in} - V_{out})D_{\max}}{\Delta I_{\min} \cdot f_s}, \tag{3}$$

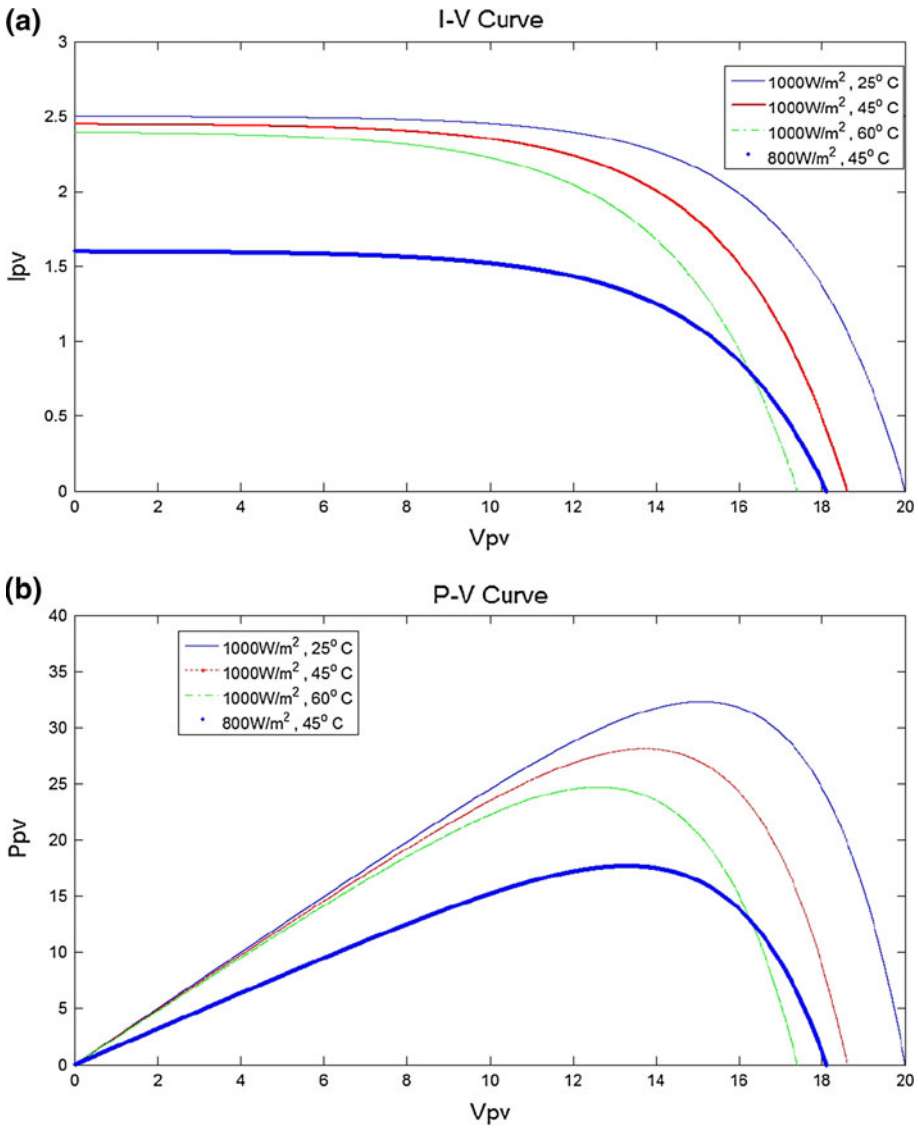

Fig. 3 **a** I–V curves and **b** P–V curves of the photovoltaic array

where D_{max} is the duty cycle at maximum converter output power; ΔI_{min} is the peak-to-peak ripple of the inductor current; f_s is switching frequency. The output capacitance is next calculated to offer a desired peak-to-peak output voltage ripple (V_{rip}) which should be less than 1 %. The output voltage ripple and output capacitance can thus be designed by

$$V_{rip} = 0.01 \cdot V_{out}, \tag{4}$$

$$C_{out} \geq \frac{Q}{V_{rip}} = \frac{\Delta I}{8 f_s V_{rip}}, \tag{5}$$

where Q is the electric charge; ΔI is the peak-to-peak ripple of the capacitor current.

The specification of the buck converter in this study is listed in Table 1. The range of duty cycle ratio considering a finite range of possible input voltage (V_{in}) spans between

$$D_{\max} = \frac{V_{out} + V_D}{V_{in,\min}} \cdot 100\ \% = \frac{4.2 + 0.7}{10} \cdot 100\ \% = 49\ \%, \tag{6}$$

$$D_{\min} = \frac{V_{out} + V_D}{V_{in,\max}} \cdot 100\ \% = \frac{4.2 + 0.7}{32} \cdot 100\ \% = 15.31\ \%, \tag{7}$$

where V_D is the voltage of the diode. In this study, the peak-to-peak ripple of the inductor current is assumed to 10 %, thus

$$\Delta I_{\min} = 2 \cdot 0.1 \cdot I_{out,\max} = 0.58\ \text{A}, \tag{8}$$

where $I_{out,max}$ is the maximum output current. The output voltage ripple V_{rip} can be calculated by

$$V_{rip} = 0.01 \cdot V_{out} = 42\ \text{mV}. \tag{9}$$

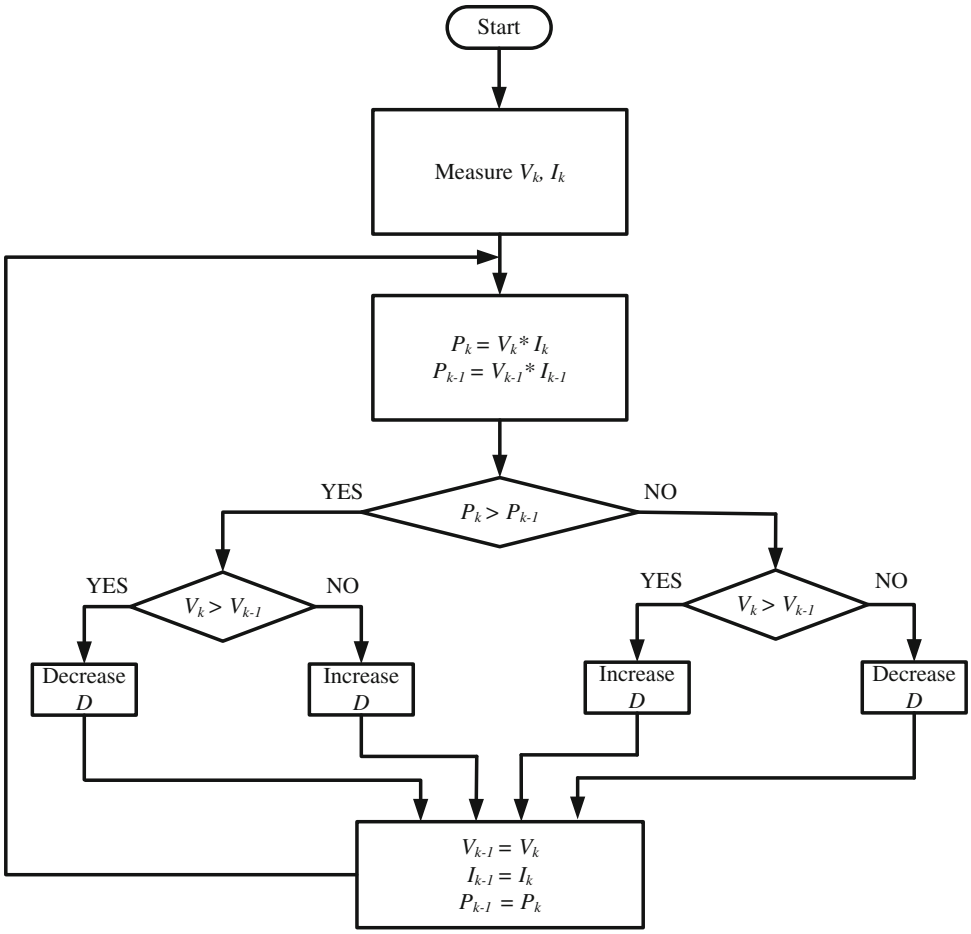

Fig. 4 The computation flow-chart of the MPPT algorithm

The inductance L can be then calculated by Eqs. (3), (6) and (8) with those given in Table 1 as

$$L > \frac{(V_{in} - V_{out})D_{\max}}{\Delta I_{\min} \cdot f_s} = \frac{(10 - 4.2) \cdot 0.49}{0.58 \cdot 40k} = 122.5\ \mu\text{H}. \tag{10}$$

The capacitance C_{out} can be then calculated by Eqs. (5), (8) and (9) with those in Table 1 as

$$C_{out} \geq \frac{Q}{V_{rip}} = \frac{\Delta I_{\min}}{8 f_s V_{rip}} = \frac{0.58\ \text{A}}{8 \cdot 40\ \text{kHz} \cdot 42\ \text{mV}} = 43.15\ \mu\text{F}. \tag{11}$$

The overall system circuit designed is shown in Fig. 7. The determined inductances and capacitances would be later used for realizing the buck DC–DC converter.

3 Battery charger

State of charge (SOC) serves well as an indicator for current battery capacity. SOC depends mainly on battery's internal chemical reaction (Jianwei et al. 2012). This study proposes a fast battery charging algorithm that does not only prolong battery lifetime by restoring the maximum battery SOC in the shortest time but also with the temperature compensation. The designed charging algorithm consists of three different stages, namely constant current (CC), pulse charging and trickle charging. In this study, a lithium-ion battery from RPC Corporation is considered for exemplary study, the characteristics of which are given in Table 2 (http://www.rpc.com.tw).

3.1 Models for a lithium-ion battery

The electro-chemical behavior of a lithium-ion battery should are different for charging and discharging, to thus, to characterize battery completely, two models for charging and discharging should be prescribed. Figure 8 shows the complete models of a lithium-ion battery where $u(t)$ is used to switch between charge and discharge mode. The proposed discharge model is similar to the Shepherd model (Edrington et al. 2010) but can represent accurately the voltage dynamics with the battery current varying. The battery voltage obtained is given by

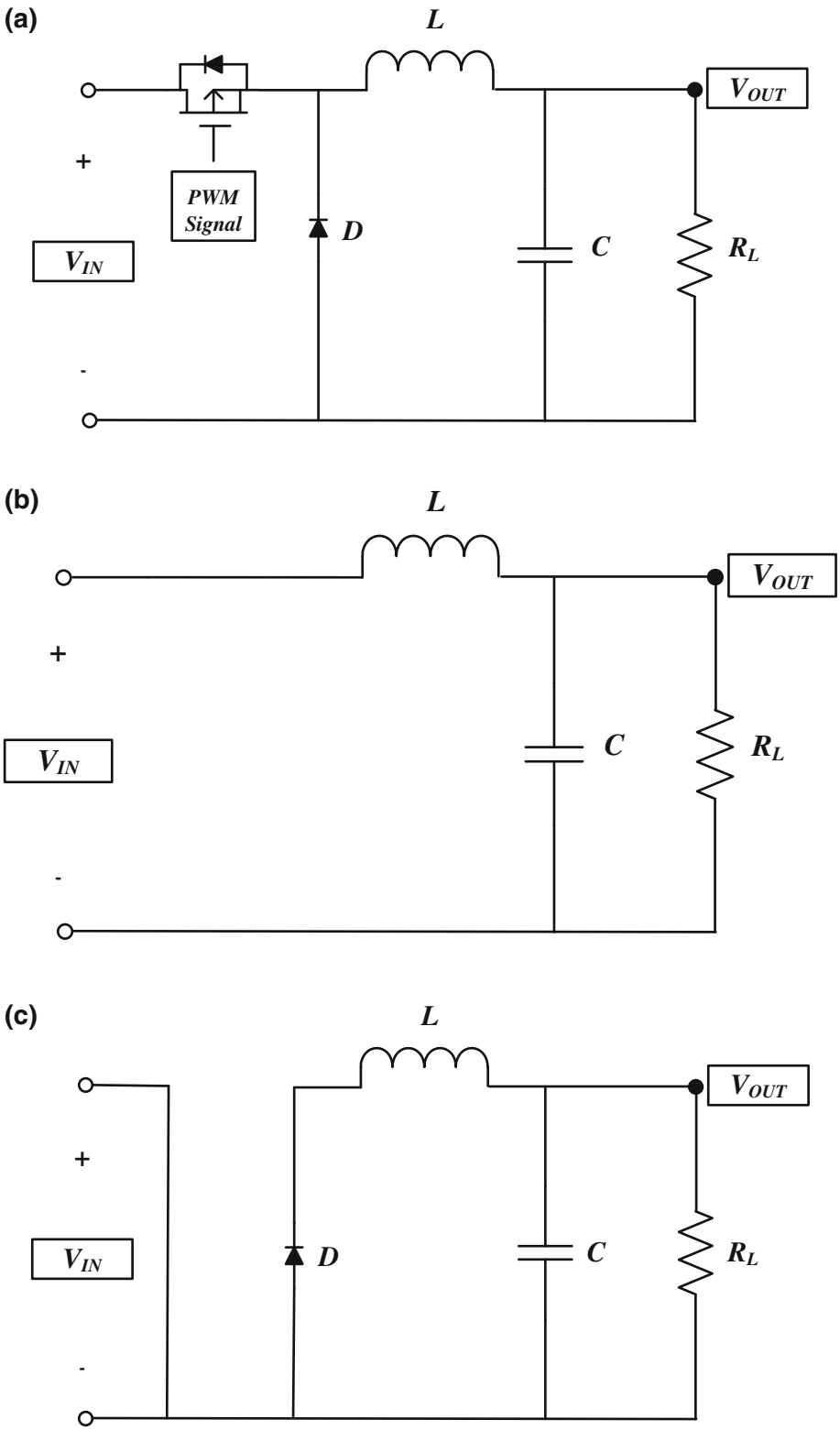

Fig. 5 **a** The buck DC–DC converter circuit; **b** the equivalent circuit when the power switch closed; **c** the equivalent circuit when the power switch open

$$V_{bat} = E_0 - K \cdot \frac{Q}{Q - it} \cdot it - K \cdot \frac{Q}{Q - it} \cdot i^* - R \cdot i + A \cdot \exp(-B \cdot it), \quad (12)$$

where V_{bat} is battery voltage; E_0 is the battery open circuit voltage when fully charged; K is polarization resistance; Q is battery capacity; it is actual battery charge; A is exponential zone amplitude; B is exponential zone time

constant inverse; R is internal resistance; i is battery current; i^*i^* is filtered current. The particularity of this model is to use a filtered current (i^*i^*) to flow through the polarization resistance. The open circuit voltage varies non-linearly with the SOC. This phenomenon is modeled by the polarization voltage term [the second term in Eq. (12)]. Note also in Eq. (12) that different from Shepherd model, an additional term concerning the polarization voltage is added to better represent the open circuit voltage behavior, while another concerning the polarization resistance [the third term in Eq. (12)] is slightly modified.

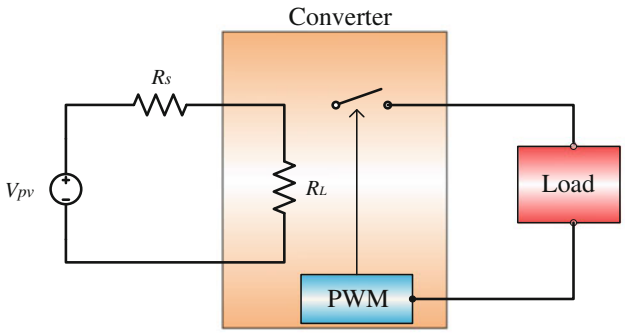

Fig. 6 Impedance matching

Table 1 The specification of the DC–DC buck converter

Parameters	Value
Input voltage (V_{in})	10–26 V
Output voltage (V_{out})	4.2 V
Output current (I_{out})	2.5 A
Switching frequency (f_s)	25 kHz

In the charge mode, the voltage increases rapidly when the battery reaches the full charge that is modeled by the polarization resistance term in Eq. (12). The polarization resistance increases until the battery is almost fully charged ($it = 0$). Instead of the discharge model from Eq. (12), the polarization resistance for charge mode is now given by

$$Pol.R = K \cdot \frac{Q}{it}. \tag{13}$$

The polarization resistance increases abruptly when the battery almost reached fully charged status. Form Eq. (13), the polarization resistance is infinite when the battery is fully charged. That is not possible in a real battery. In fact, the contribution of the polarization resistance is often deviated in reality by about 10 % from the full capacity of the battery. Thus, the polarization resistance in Eq. (13) can be rewritten to

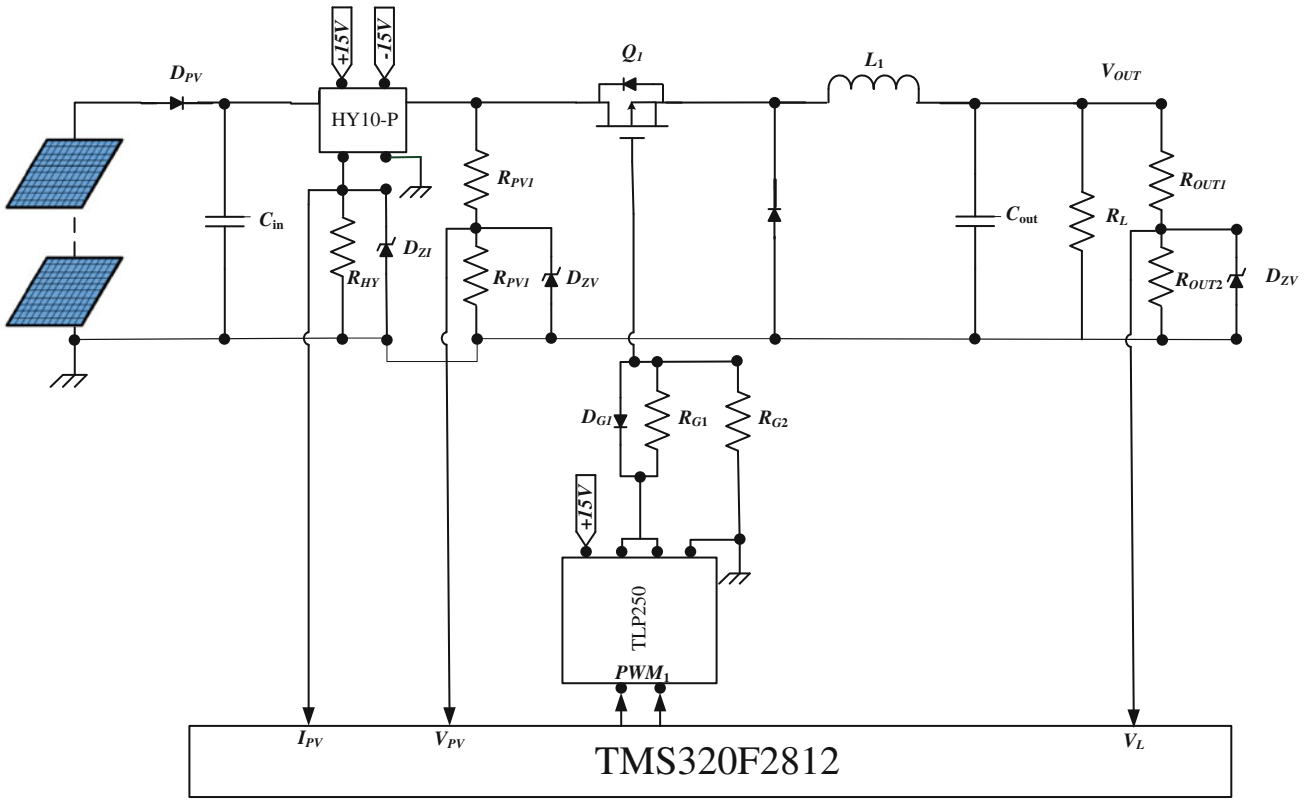

Fig. 7 The overall photovoltaic system

Table 2 Specifications of the adopted lithium-ion battery

Item	Specification	Remark
Nominal capacity	4,000 mAh	0.2 C discharge
Nominal voltage	3.7 V	
Cut-off voltage	3 V	
Charge current (Std.)	0.2 C mA	0 to +40 °C
Charge current (Max.)	1 C mA	0 to +40 °C
Charge voltage	4.2 ± 0.03 V	
Charge time (Std.)	6–7.0 h	
Charge time (Max.)	2–3.0 h	
Discharge current (Std.)	0.2 C mA	−20 to +60 °C
Discharge current (Max.)	1 C mA	−20 to +60 °C
Internal resistance	<18 mΩ	AC impedance 1 kHz

$$Pol.R = K \cdot \frac{Q}{it - 0.1Q}. \tag{14}$$

With Eq. (14), the charge model could be represented by

$$V_{bat} = E_0 - K \cdot \frac{Q}{Q - it} \cdot it - K \cdot \frac{Q}{it - 0.1Q} \cdot i^* - R \cdot i + A \cdot \exp(-B \cdot it). \tag{15}$$

To this point, the charge and discharge models are successfully obtained. The associated charging method with temperature compensation is designed and presented in the next section.

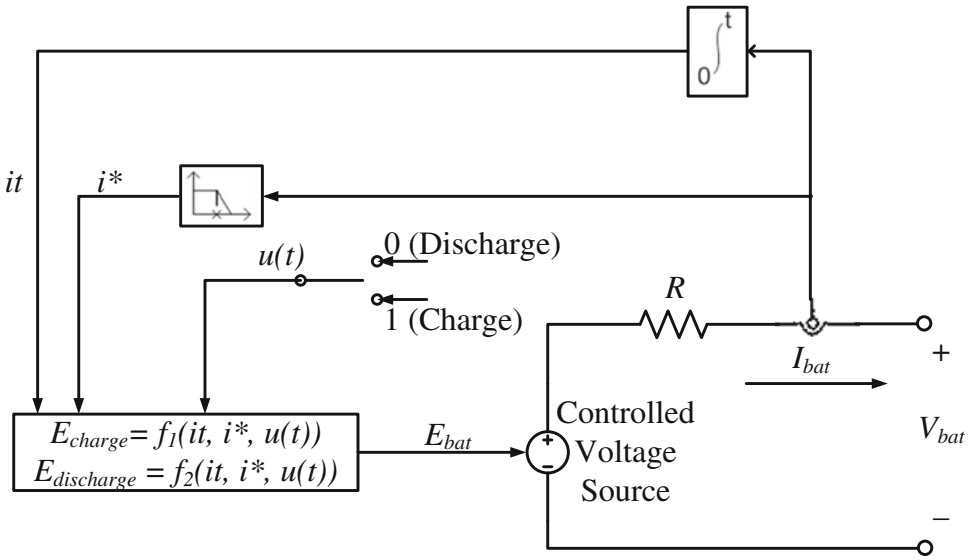

Fig. 8 Models of the lithium-ion battery

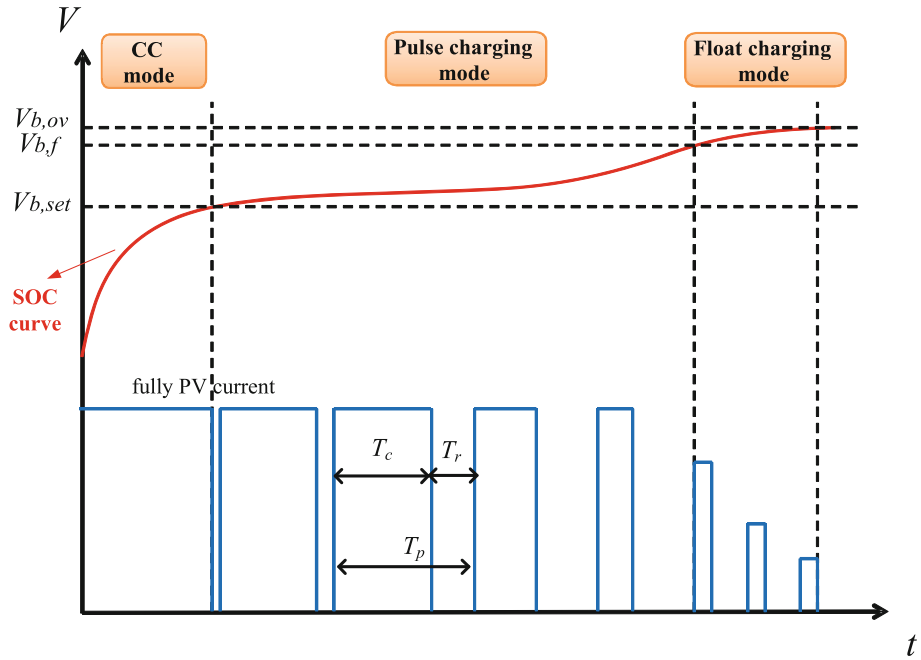

Fig. 9 Illustration of the proposed charging modes

3.2 Charging method

The proposed charge method consists of three different stages, i.e., constant current (CC), pulse charging and floating (trickle) charging, as illustrated in Fig. 9. In the CC mode, the current at maximum power of the PV array is used for fast charging. The temperature of battery normally rises rapidly in this mode. In order to avoid large temperature rise that possibly damages the battery, the pulse charging mode is adopted subsequently to slow down temperature rise while maintaining relatively fast charging speed. To prevent battery damage by charging as battery capacity is close to its full status, the float charging mode is finally activated by further decreasing charging currents. The charge algorithms associated with the above-mentioned three different approaches are designed herein with capabilities to regulate charging current to desired values. The mechanism depends on the feedback parameter of voltage, capacity and temperature of the battery. The details of the algorithms are given in the followings.

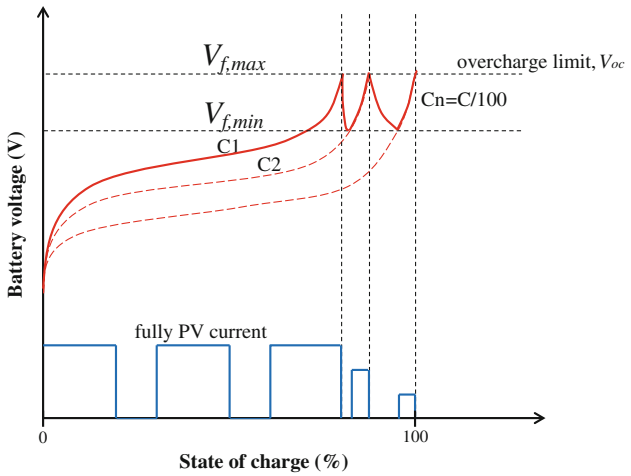

Fig. 10 Illustration of the proposed trickle charging

As the battery voltage is less than $V_{b,set}$, the CC charging mode with the current achieving MPP of the PV array is adopted for fast charging. When the battery voltage is between $V_{b,set}$ and $V_{b,f}$, the pulse charging mode is employed to avoid undesired temperature rise. $V_{b,set}$ is a pre-set voltage defining boundary to change from CC to pulse charging modes. $V_{b,f}$ is the nominal voltage for full battery capacity. $V_{b,ov}$ is the overcharge voltage limit. Both charge currents for the CC and pulse charging modes are at maximum powers of the PV array. The charge period (T_c) of pulse charging mode is determined by proportionality to the battery voltage. The electrolysis reaction of the battery is relaxed during the rest period T_r to slow down battery temperature rising. The charge period T_c and the rest period T_r are determined by the sensed battery voltage as follows (Ting-Peng et al. 2010),

$$T_c[k] = T_p - \left(\frac{V_b[k] - V_{b,set}}{V_{b,f} - V_{b,set}} \cdot 0.4T\right), \tag{16}$$

$$T_r[k] = T_p - T_c[k], \tag{17}$$

$$V_{b,set}[k] = V_{b,set}[k-1] + (T_a - 25)N_c \cdot \alpha, \tag{18}$$

$$V_{b,f}[k] = V_{b,f}[k-1] + (T_a - 25)N_c \cdot \alpha, \tag{19}$$

where T_a is the ambient temperature; T_p is the period of pulse charging; N_c is the number of cells of battery stack; V_b is the battery voltage; α is temperature compensation coefficient. The battery temperature could be suppressed by adjusting T_c. The trickle charging method (Koutroulis and Kalaitzakis 2004), as illustrated by Fig. 10, is used in the float charging

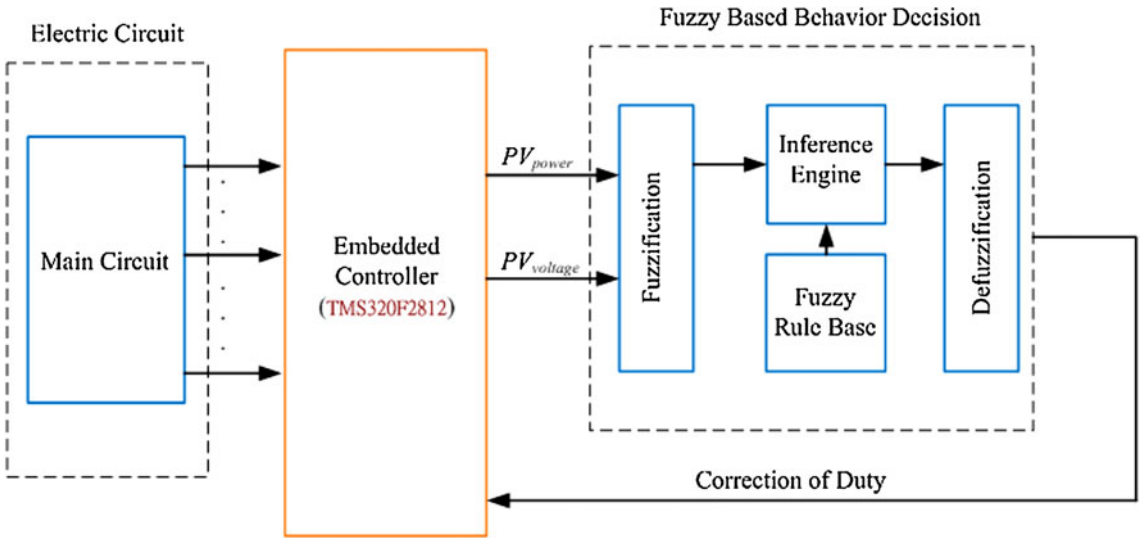

Fig. 11 The fuzzy battery-managing controller (FBMC) in blocks

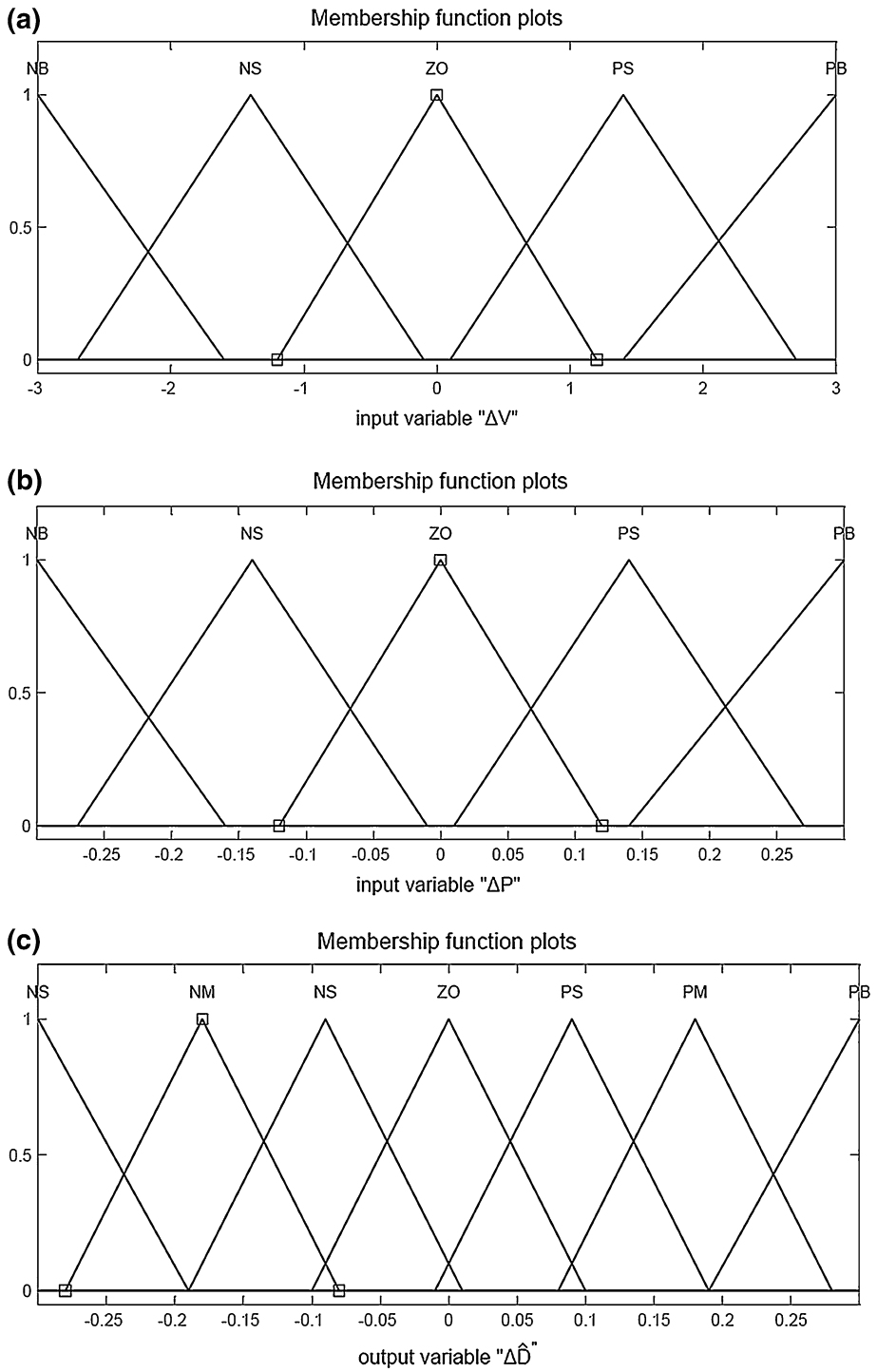

Fig. 12 The membership functions prescribing variations of **a** input voltage; **b** input power; **c** output duty cycle

mode to achieve 100 % SOC. In this method, the charging current is switched between on and off, the battery reaches $V_{f,min}$ and $V_{f,ma}$, respectively. Also the charging current is decreased from C1, C2, …, to Cn = C/100 for battery to reach realistic full capacity—100 % SOC. $V_{f,min}$ and $V_{f,max}$ are adjusted according to battery temperature

$$V_{f,\min} = 4.2 + (T_a - 25)N_c \cdot \alpha, \tag{20}$$

$$V_{f,\max} = 4.23 + (T_a - 25)N_c \cdot \alpha, \tag{21}$$

where $V_{f,min}$ and $V_{f,max}$ are set as the nominal voltage and overcharge voltages of battery, respectively. By the proposed three charging methods, the battery capacity should

be able to reach its realistic full level without intolerable temperature rise.

4 Fuzzy battery managing controller

An intelligent MPPT controller is designed to manage the switching in the buck converter for arbitrary levels of solar exposure and environment temperature of the photovoltaic (PV) panel. The intelligence of MPPT is achieved by a fuzzy mechanism. The controller is thus named Fuzzy Battery Managing Controller (FBMC). The goals of FBMC are twofold: one is the MPPT when the battery condition is in the CC and pulse charging mode. In fact, when the battery is in the mode of pulse charging, the MPPT is also active within pulse durations, which is determined by Eq. (16). Design of FBMC for MPPT is illustrated by Fig. 11, where the fuzzy mechanism includes three blocks—fuzzification, interference rules and defuzzification.

Table 3 Table of designed fuzzy rules

ΔP	ΔV				
	NB	NS	ZO	PS	PB
NB	NB	NM	NS	PM	PB
NS	NM	NS	ZO	PS	PM
ZO	NS	ZO	ZO	ZO	PS
PS	PM	PS	ZO	NS	NM
PB	PB	PM	PS	NM	NB

4.1 Fuzzification

The first phase of computation for a fuzzy controller is fuzzification, which is started with choosing the output voltage (V_{pv}) and power (P_{pv}) of the PV array as the two input variables of the fuzzy controller to be designed, since the PV voltage is adjusted to reach maximum power during MPPT. The adjustment increment on V_{pv} is tuned based on the instantaneous value of P_{pv}. In this way, two sets of membership functions are defined for variations of the output voltage (denoted by ΔV) and power (denoted by ΔP) of the PV array, respectively, as shown in Fig. 12. On the other hand, the output of the controller is the variation on duty cycle of the switch (denoted by $\Delta\hat{D}$) for the buck converter. The fuzzification on the aforementioned input and output variables next carried out by seven fuzzy sets as NB, NM, NS, ZE, PS, PM, PB in the triangle membership functions as shown in Fig. 12. The range for input ΔV is chosen from -3 to 3. The range for input ΔP is defined

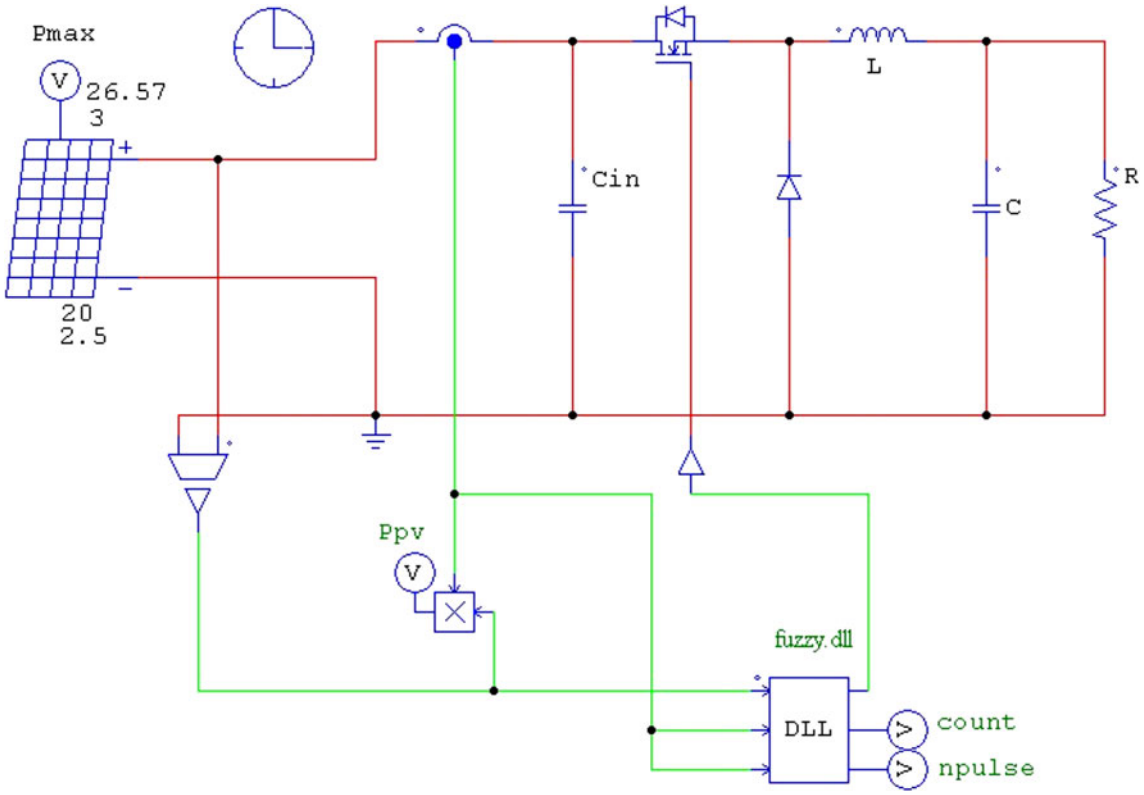

Fig. 13 The circuit model established by Powersim

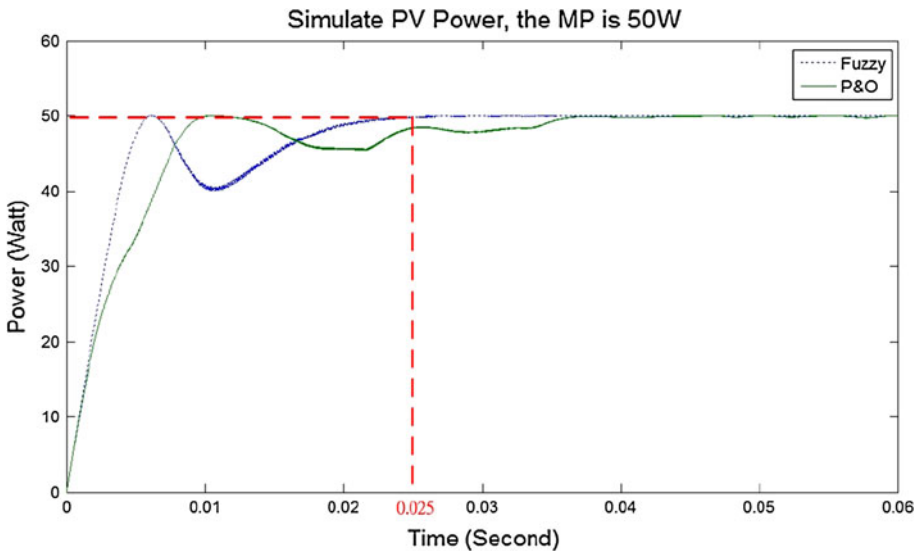

Fig. 14 Simulation results of the output power of the PV array by the P&O method and FLC

Table 4 Specifications of the adopted PV array

Parameters	
Maximum power rating (P_{max})	50 W
Rated current (I_{mp})	2.5 A
Rated voltage (V_{mp})	20 V
Short-circuit current (I_{sc})	3 A
Open-circuit voltage (V_{oc})	26.57 V
Temp. coefficient: short-circuit current	2.06 mA/°C
Temp. coefficient: open-circuit voltage	−0.77 V/°C

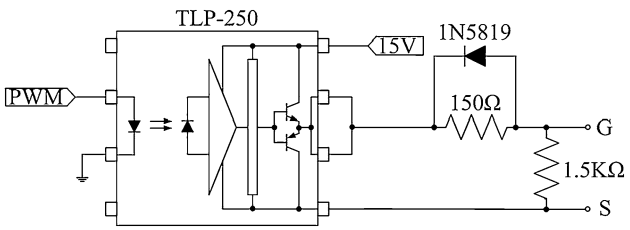

Fig. 15 The isolated gate driver circuit

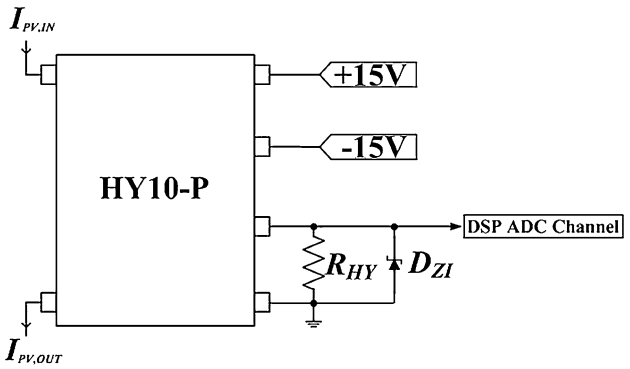

Fig. 16 The hall current sensing circuitry

from −0.3 to 0.3. The range for output $\Delta\hat{D}$ is defined from −0.3 to 0.3.

4.2 Fuzzy rule base and fuzzy inference

With memberships defined, linguistic rules for the fuzzy controller are determined based on the rules in fact equivalent to those described in Fig. 4 for the aforementioned P&O method. This would lead the operating point of the PV array to approach the maximum power point. Even with the same linguistic rules, the FBMC controller proposed herein is considered more advanced than the conventional P&O method due to its capability to continuously tune the level of duty increment via the mechanism of fuzzification, interference and defuzzification. The IF–THEN rules of fuzzy control for the four conditions following the flow chart of control algorithm in Fig. 4 could be expressed as

$$IF\ \Delta P<0\ and\ \Delta V<0,\ THEN\ \Delta\hat{D}<0; \tag{22}$$

$$IF\ \Delta P<0\ and\ \Delta V>0,\ THEN\ \Delta\hat{D}>0; \tag{23}$$

$$IF\ \Delta P>0\ and\ \Delta V<0,\ THEN\ \Delta\hat{D}>0; \tag{24}$$

$$IF\ \Delta P>0\ and\ \Delta V>0,\ THEN\ \Delta\hat{D}<0. \tag{25}$$

The associated rule table is shown in Table 3, which enables a continuous, smooth adjustment on the duty increment $\Delta\hat{D}$.

4.3 Defuzzification

Having forged fuzzy interference scheme, linguistic output variables need to be converted into numerical values. The subsequent defuzzification is carried, which is in fact an inverse transformation of fuzzification. It maps the output

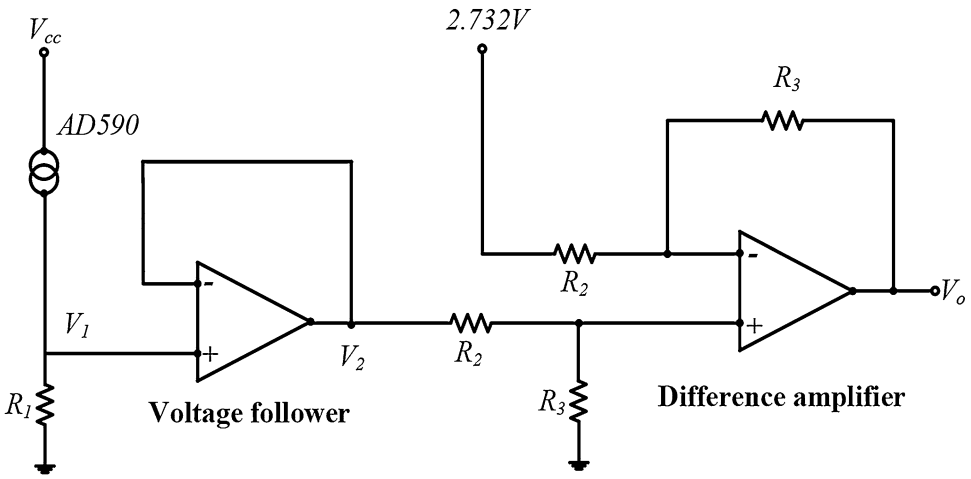

Fig. 17 The temperature-sensing circuit

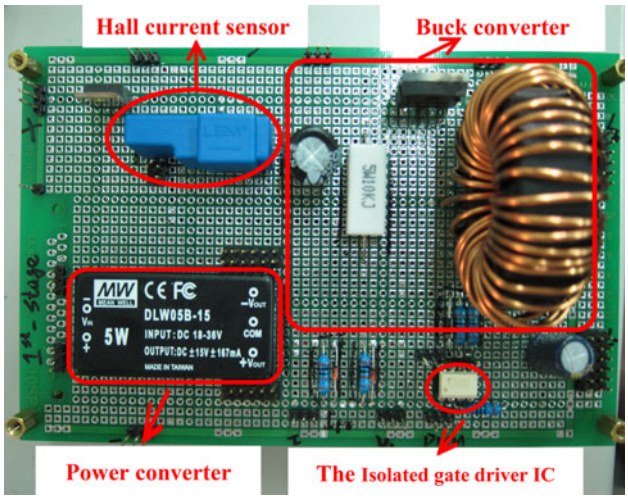

Fig. 18 The implemented circuit board for a single-stage DC–DC converter

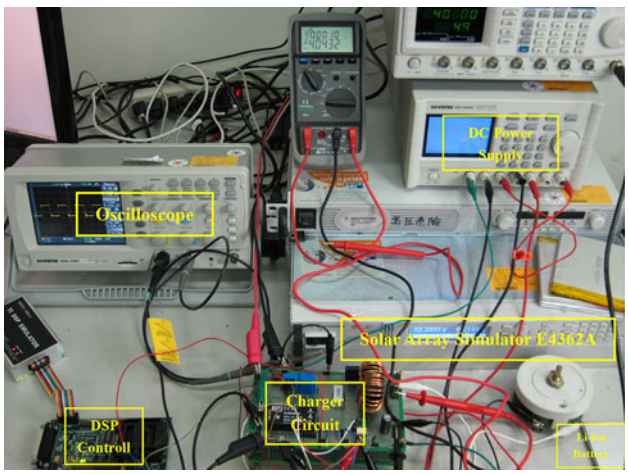

Fig. 19 The entire experimental testing system

from the fuzzy domain back into the numerical domain. The center average method is used herein for defuzzification, which could be expressed as

$$\Delta\hat{D} = \frac{\sum_{i=1}^{4} W_i \times \Delta D}{\sum_{i=1}^{4} W_i}, \tag{26}$$

where W is the height of fuzzy set and ΔD is the center of area of fuzzy set.

5 Simulation and experiments

With system models established and controllers deigned, simulations and experiments are conducted to tune controller parameters and validate the expected performances of simultaneous MPPT and battery charging by the proposed FBMC.

5.1 Simulation results

The system modeling for circuit simulation carried out by the available software Powersim is shown in Fig. 13. The parameters of the buck converter is designated as those practical values adopted in the experiment, i.e., L is 1.5 mH; C is 400 μF and R is 5Ω. Note that these passive components are chosen in satisfying design criteria distilled by Eqs. (10) and (11). The afore-mentioned MPPT methods of P&O and the proposed FLC are realized and embedded into the block DLL in this figure by C language. Comparison is made between the two methods of P&O and FLC in term of the performance in MPPT. Figure 14 presents varied simulation results by Powersim for MPPT in terms of the power extracted from the PV panel, where the specification of considered PV array is shown Table 4. The finally-found maximum power point (MPP) is at 50 Watt with V_{MPP} at 20 V and I_{MPP} at 2.5 A. It is seen from this

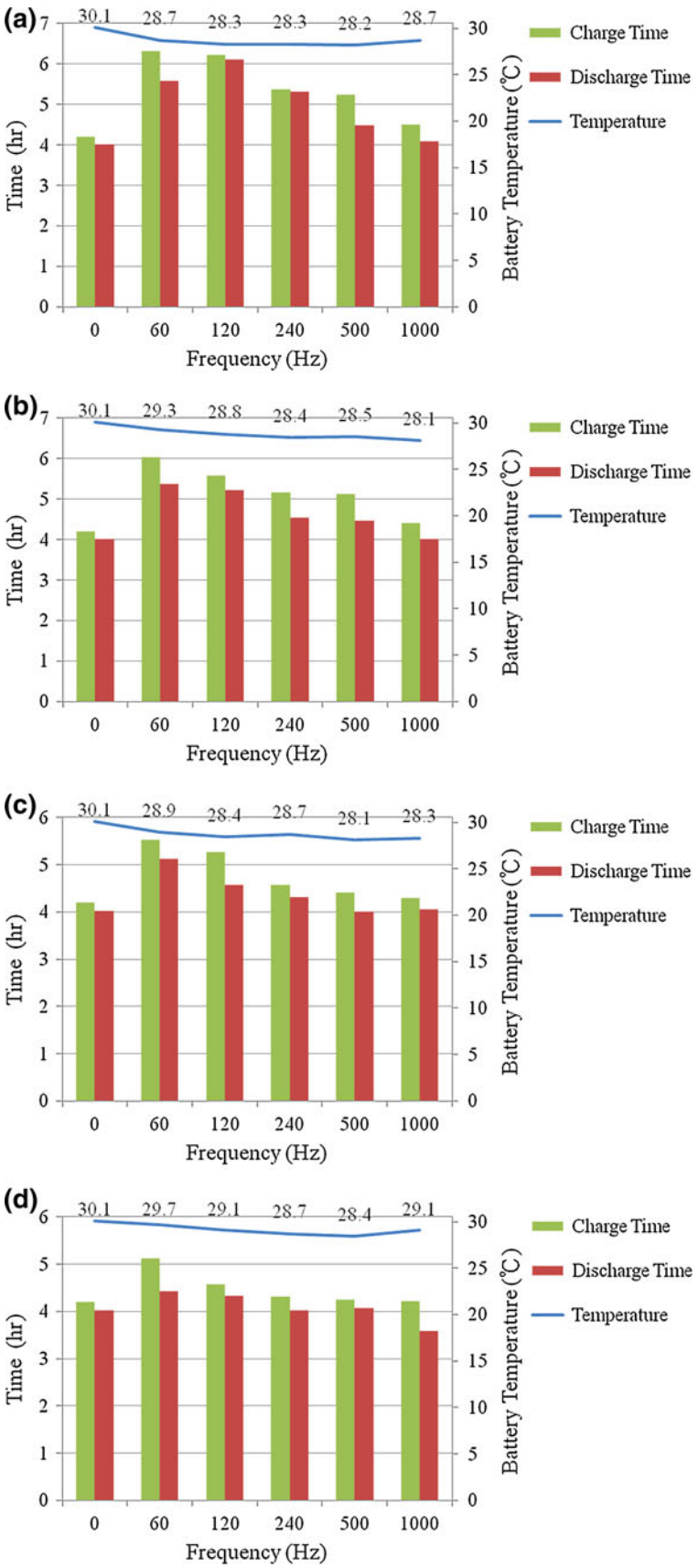

Fig. 20 Resulted charge/discharge durations for different frequencies. **a** Duty cycle is 60 %; **b** 70 %; **c** 80 %; **d** 90 %

figure that MPP is achieved by the proposed FLC within a short period of 0.025 s, while much more oscillation occurs for the P&O method employed than FLC, not only in transient but also in the steady state periods. The designed FLC could track the MPP in a faster pace with high precision than P&O. In a short conclusion, the simulation results show that the proposed FBMC with the proposed buck converter and the PV system can track the MPP efficiently and effectively in a real-time fashion.

5.2 Experimental validation

5.2.1 Experimental setup

An experiment system as shown in Fig. 7 is established for validating the expected performance of the designed controller and the buck DC–DC converter. It includes a 32-Bit microprocessor of DSP (TI TMS320F2812), an optical coupler circuit and a current sensor (HY-10P). The aforementioned DSP chip of TMS320F2812 is a stand-alone module which features a 150 MHz clock, a high-performance 32-Bit processor, and 12-bit ADC output. The optical coupler is an isolating device consisting of a transmitter and a receiver, through which the electrical signal is converted to a light beam, transferred, then converted back to an electrical signal. In this way, electromagnetic interference and undesired electrical pulsations could be isolated to the DSP module. Note that an optical isolator is usually regarded as a single integrated package, but the opto-isolation can also be achieved by using separate devices. Digital opto-isolators modify the state of their outputs when the input state changes. Analog isolators produce an analog signal which reproduces the input. Figure 15 shows the circuit design insight of the isolated gate driver. In addition, the diode (1N5819) is adopted to improve the falling transient time with the optical coupler, which accelerates the charge into ground. Finally, the hall current sensor (HY-10P) is used to sense the electrical current from the photovoltaic panels. Figure 16 shows the circuitry associated with the hall sensor that connects the resistance from the output of HY-10P into ground and in a parallel fashion with a Zener diode to limit the output voltage under 3 V. This avoids the breakdown of the analog to digital channel (an ADC) of DSP (TMS320F2812). In addition, an external circuit, a temperature-sensing circuit, is used to sense the battery temperature continuously in an on-line fashion, as shown in Fig. 17. The temperature sensor AD590 is a 2-terminal integrated transducer that produces an output current proportional to absolute temperature. This AD590 acts with a high impedance that offers 1 μA per an increment of 1°K. V_1 is seen as an output of a voltage divider with AD590, thus,

$$V_1 = (273.2\ \mu\text{A} + T)R_1. \tag{26}$$

A voltage follower is subsequently used to transfer V_1–V_2, which also overcomes effects of load variation. Finally, the output V_o is amplified by a difference amplifier circuit by

$$V_o = (V_2 - V_{ref})\frac{R_3}{R_2}. \tag{27}$$

By the above design, the output voltage increases by 50 mV when the temperature rises by 1 °C using the designed temperature sensing circuit.

The voltage and current of the PV module are sensed by an optical coupler circuit and a current sensor, respectively. The sensed signals of voltage and current are used as the inputs to the FBMC. Figure 18 gives a photo showing the implementation of the designed circuit for the buck DC–DC converter. Figure 19 shows the entire testing system, where a photovoltaic (PV) panel is replaced by the Agilent Solar Array Simulator (E4362A), which is a 600w PV simulator, and a direct-current power module that simulates the output characteristics of a photovoltaic (PV) string. This E4362A is in fact a current source with a low output capacitance that offers changes in current–voltage curve to allow users to accurately simulate the output of different PV strings under various environmental conditions. Four key operational parameters $\{V_{OC}, I_{SC}, V_{MP}, I_{MP}\}$ are needed for the PV simulator to create a characteristic curve of a PV string. V_{OC}, I_{SC}, V_{MP} and I_{MP} are open-circuit voltage, short-circuit current, voltage at MPP and current at MPP, respectively.

5.2.2 Experiment results

In order to find the appropriate charging frequency, duty cycle of switching for the designed buck converter is fixed while recording the battery temperature, charge time and discharge time in difference frequencies. The results with duty cycles of 60, 70, 80 and 90 % are considered and shown in Fig. 20. Note that the charge current is 2A. The

Table 5 Comparison of charging durations between the proposed pulse charging method and a general pulse charging method

	Frequency = 240 Hz				
	Baseline pulse charging method				The proposed method
Duty cycle (%)	60	70	80	90	Variable
Charge time (h)	5:38	5:17	4:58	4:31	4:48
Discharge time (h)	5:21	5:54	4:22	4:12	4:31
Temperature (°C)	28.4	28.4	28.7	28.7	28.3

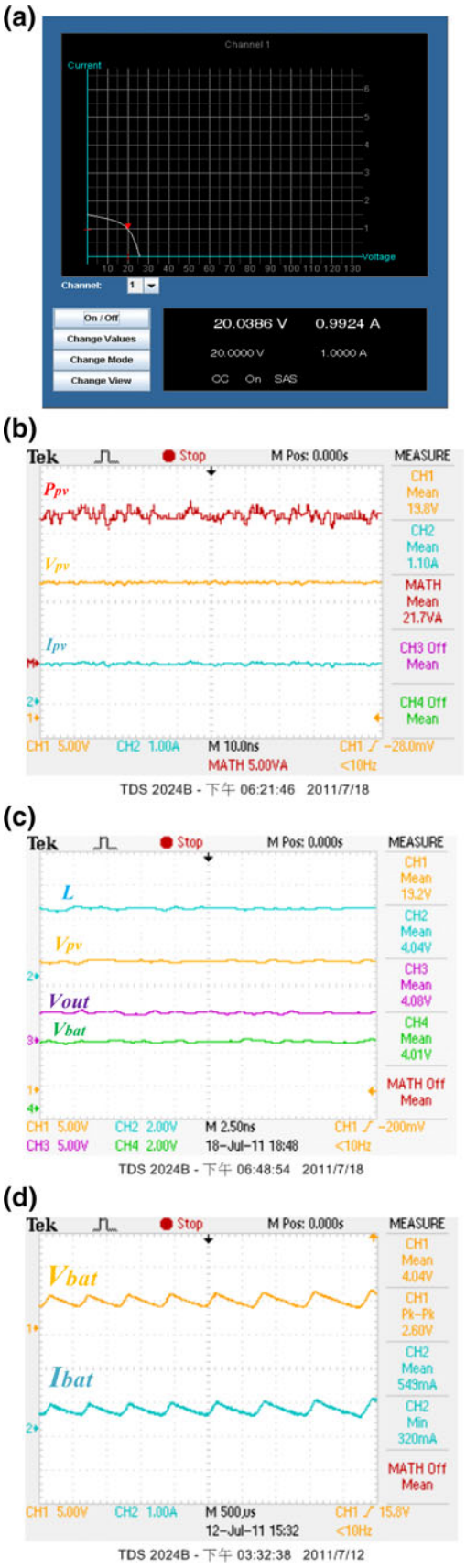

◀**Fig. 21** Experimental results by the PV panel ($V_{OC} = 26$ V, $I_{SC} = 1.5$ A, $V_{MP} = 20$ V, $I_{MP} = 1$ A); **a** Agilent web control; **b** waveforms (V_{PV}, I_{PV}, P_{PV}); **c** output voltage waveforms; **d** battery voltage and current in the pulse charging mode

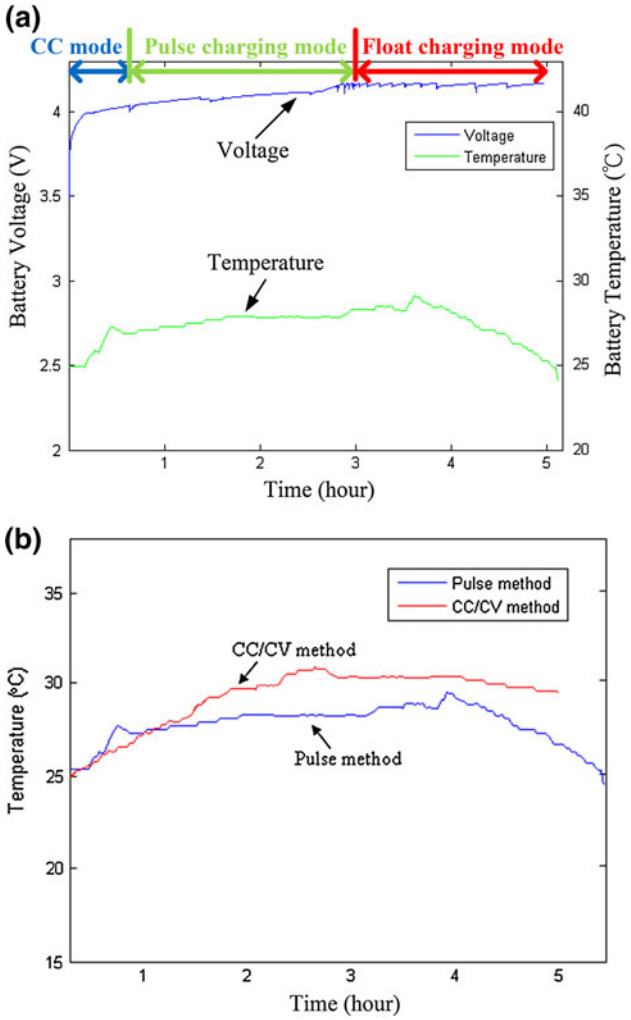

Fig. 22 **a** Evolutions of battery voltage and temperature during battery charging. **b** Comparison of temperature evolution between the proposed pulse charging method and a general CC/CV method

charge time, low temperature and charge capacity (equivalent to discharge time in Fig. 20) are all considered conditions to the best switching frequency of the converter. Those results show that the charge capacity in low switching frequency (60–240 Hz) is higher than high switching frequency (500–1 kHz) as also for the discharge time. Considering all experimental data presented in this figure, 240 Hz appears to be the best frequency. The comparison between methods of the designed pulse charging and baseline fixed pulse charging are shown in Table 5. In the designed pulse charging method, the initial charge duty (T_c) is 90 % for reducing the charging time. By

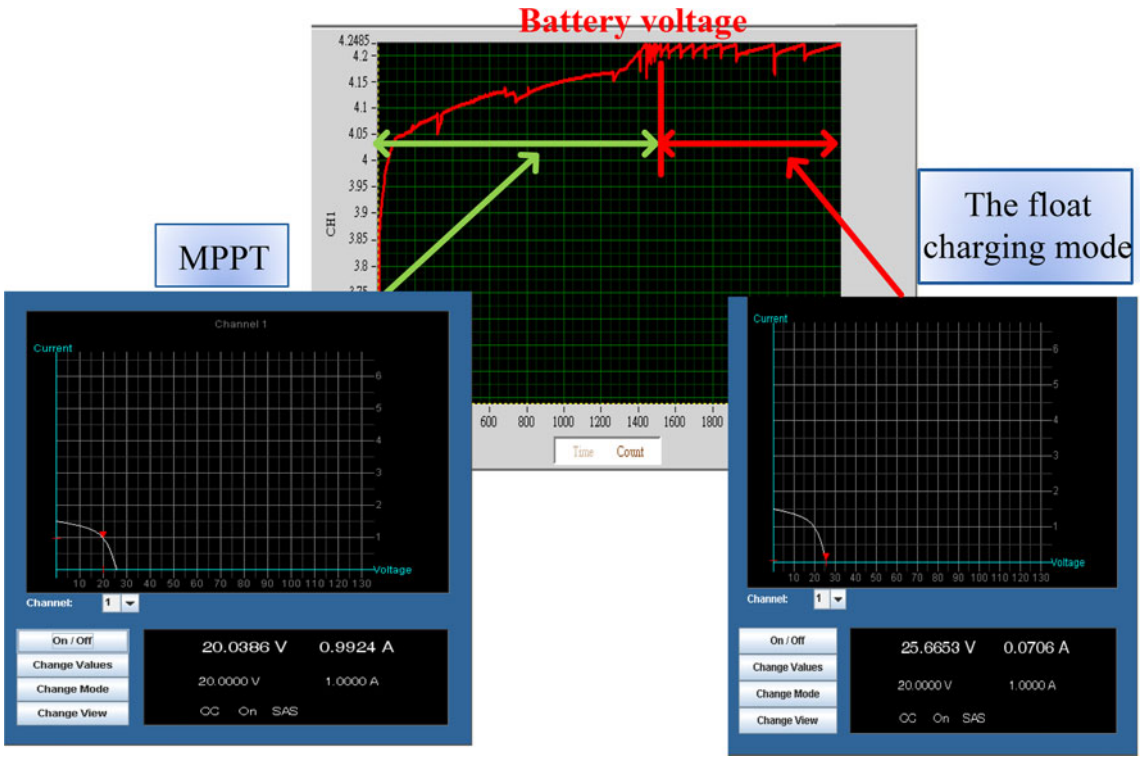

Fig. 23 The entire operation process of the PV array in different modes

Eq. (16), the charge duty is reduced to slow down the battery temperature increase.

Figure 21 shows the experiment results by first setting the open circuit voltage V_{oc} of the PV-string simulator E4362A at 26 V, short circuit current I_{sc} 1.5 A, maximum power voltage V_{MP} 20 V and the maximum power current I_{MP} 1 A. Figure 21a is the machine interface of the Agilent web control, which is provided by the simulator E4362A, where is seen for this case an I–V curve of a PV panel. The red point is the instantaneous operating point of the PV array in terms of current and voltage. With the designed FBMC controller implemented by the DSP module in operation, the operating point (red dot) is successfully stabilized after some period of time to MPP. Various signals at stabilization is shown in Fig. 21b. The output power is maximized to approximate 20 W when the current and voltage of the PV panel reaches 1A and 20 V, respectively, actually corresponding to the location of the red dot in Fig. 21a. Note that noises are observed in various signals which are possibly resulted from ADC and/or environment. Figure 21c shows the output voltage waveforms of the adopted DC–DC converter, where the output voltage is stabilized at 4.08 V, showing the capability of the designed controller and circuit topology to provide a constant output and maximum power output from the PV panel. The waveforms of the voltage and current of the battery in the pulse charging mode are shown in Fig. 21d. Integral results for battery charging are shown in Fig. 22 of which charge current for constant current is 3A. The voltage curve is seen as a typical one experiencing modes of constant current (CC) charge, pulse charge and trickle charge/discharge. It is also seen from this figure that the total charge time is close to 5 h. The temperature resulted from the proposed charging method is lower than a general CC/CV method. Figure 23 shows the corresponding statuses of the adopted PV array in different modes. In this figure, the displayed battery voltage experiences different charging stages from modes of MPPT (including CC and pulse charging) to floating charge. Note that the charging current during pulse-charging is the same as that MPP (I_{MP}) until the battery voltage reaches to pre-designated float voltage ($V_{b,f}$), then the supply current of the PV array is reduced gradually in the float charging mode until the charge rate is reached to $C/100$ to maximize battery capacity. The above proposed charging scheme successfully contains battery temperature as shown in Fig. 22b.

6 Conclusion

A buck DC–DC converter responsible for extracting solar energy of a photovoltaic (PV) panel is proposed in this study. The converter is equipped with a fuzzy mechanism for maximum power point tracking (MPPT) and a function

of temperature compensation of a battery charger. Modeling and simulation on the PV system and the DC–DC converter circuit are carried out by the software Powersim. The proposed temperature compensation model with the pulse charging method is used to achieve fast charging and contain the temperature rising. Simulations are intended to validate the performance of the proposed fuzzy battery-managing controller (FBMC). It is shown that the tracking process for the maximum power point is as fast as within 0.015 s, which is also proven in a much faster and stable pace with designed FBMC as compared to conventional P&O method. Experiments are carried out to validate the expected performance of the designed FBMC controller and the buck converter. It is shown that a fast battery charging is well achieved with the chosen charge frequency 240 Hz, while the temperature can be contained effectively with the designed pulse-charging method. In the charging process, a fast MPPT is made possible by the designed FBMC in both CC and pulse-charging modes. In short, the designed PV system with the proposed FBMC and charging method is proven working effectively towards battery fast charging and temperature compensation.

Acknowledgments The authors appreciate the support from National Science Council of R.O.C under the grant no. NSC 100-2221-E-009-091 and 101-2221-E-009-165. This work was also supported in part by the UST-UCSD International Center of Excellence in Advanced Bio-Engineering sponsored by the Taiwan National Science Council I-RiCE Program under Grant NSC-100-2911-I-009-101.

References

Agorreta JL, Reinaldos L, Gonzalez R, Borrega M, Balda J, Marroyo L (2009) Fuzzy switching technique applied to PWM boost converter operating in mixed conduction mode for PV systems. IEEE Trans Ind Electron 56(11):4363–4373

Al-Atrash H, Batarseh I, Rustom K (2005) Statistical modeling of DSP-based Hill-climbing MPPT algorithms in noisy environments, APEC 2005, vol 3, pp 1773–1777, March 2005

Azimi S, Dehkordi BM, Niroomand M (2012) An adaptive incremental conductance MPPT based on BELBIC controller in photovoltaic systems, 20th ICEE, pp 324–329

Bouchafaa F, Hamzaoui I, Hadjammar A (2011) Fuzzy logic control for the tracking of maximum power point of a PV system. Energy Procedia 6:633–642

Chian-Song C (2010) T-S fuzzy maximum power point tracking control of solar power generation systems. IEEE Trans Energy Convers 25(4):1123–1132

Edrington CS, Vodyakho O, Hacker B, Azongha S, Khaligh A, Onar O (2010) Virtual battery charging station utilizing power-hardware-in-the-loop: application to V2G impact analysis. VPPC 2010:1–6

Elgendy MA, Zahawi B, Atkinson DJ (2012) Assessment of Perturb and Observe MPPT Algorithm implementation techniques for PV pumping applications. IEEE Trans Sustain Energy 3(1):21–33

Fakham H, Di L, Francois B (2011) Power control design of a battery charger in a hybrid active PV generator for load-following applications. Ind Electron IEEE Trans. 58:85–94

Huria T, Ceraolo M, Gazzarri J, Jackey R (2012) High fidelity electrical model with thermal dependence for characterization and simulation of high power lithium battery cells. IEVC 2012:1–8

Jianwei L, Mazzola M, Gafford J, Younan N (2012) A new parameter estimation algorithm for an electrical analogue battery model, APEC 2012, pp 427–433, 5–9 Feb 2012

Joe-Air J, Tsong-Liang H, Ying-Tung H, Chia-Hong C (2005) Maximum power tracking for photovoltaic power systems. Tamkang J Sci Eng 8(2):147–153

Kish GJ, Lee JJ, Lehn PW (2012) Modeling and control of photovoltaic panels utilizing the incremental conductance method for maximum power point tracking. IET Trans Renew Power Gener 6(4):259–266

Koutroulis E, Kalaitzakis K (2004) Novel battery charging regulation system for photovoltaic applications. IEE Proc Elect Power Appl 151(2):191–197

Kularatna N (2010) Rechargeable batteries and battery management systems design. IECON 2010:1–2

Kwon JM, Nam KH, Kwon BH (2006) Photovoltaic power conditioning system with line connection. IEEE Trans Ind Electron 53(4):1048–1054

Mohan N, Undeland TM, Robbins WP (2003) Power electronics, converters, applications and design, 3rd edn. Wiley, New York

Paul C-PC, Wei-Dar C, Chih-Kuo C (2012) Maximum power tracking of a generic photovoltaic system via a fuzzy controller and a two-stage DC–DC converter. Microsyst Technol 18(9–10):1267–1281

Reynaud JF, Gantet O, Aloisi P, Estibals B, Alonso C (2010) A novel distributed photovoltaic power architecture using advanced Li-ion batteries, EPE/PEMC 2010, pp S9-6–S9-12, Sept 2010

Salah CB, Ouali M (2011) Comparison of fuzzy logic and neural network in maximum power point tracker for PV systems. Electric Power Syst Res 81:43–50

Santos LJL, Antunes F, Chehab A, Cruz C (2006) A maximum power point tracker for PV systems using a high performance boost converter. Sol Energy 80(7):772–778

Szumanowski A, Yuhua C (2008) Battery management system based on battery nonlinear dynamics modeling. IEEE Trans Veh Technol 57(3):1425–1432

Taherbaneh M, Faez K (2007) Maximum power point estimation for photovoltaic systems using neural networks. ICCA 2007:1614–1619

Ta-Tau C, Ming-Ying H, Shun-Hung T, d Che-Nan L (2011) Design of digital battery charger system based on PV-module, 2011 IEEE International Conference on Fuzzy Systems, pp 1860–1865, June 2011

Ting-Peng L, Sen-Tung W, Jian-Min W, Huang-Jen C, Yu-Kang L (2010) A modular PV charger with maximum power point tracking and pulse-charging schemes. PEMD 2010:1–6

Veerachary M (2011) Fourth-order buck converter for maximum power point tracking applications. IEEE Trans Aerosp Electron Syst 47(2):896–911

Xiao W, Dunford WG, Palmer PR, Capel A (2007) Regulation of photovoltaic voltage. IEEE Trans Ind Electron 54(3):1365–1374

Yuang-Shung L, Ming-Wang C (2005) Intelligent control battery equalization for series connected lithium-ion battery strings. IEEE Trans Ind Electron 52(5):1297–1307